Control Engineering Practice ∎ (∎∎∎∎) ∎∎∎–∎∎∎

Contents lists available at ScienceDirect

Control Engineering Practice

journal homepage: www.elsevier.com/locate/conengprac

Design and control of an active knee orthosis driven by a rotary Series Elastic Actuator ☆

Wilian M. dos Santos [a], Glauco A.P. Caurin [a,b], Adriano A.G. Siqueira [a,b,*]

[a] Department of Mechanical Engineering, Engineering School of São Carlos, University of São Paulo, 13566-590 São Carlos, Brazil
[b] Center for Robotics of São Carlos and Center for Advanced Studies in Rehabilitation, University of São Paulo, Brazil

ARTICLE INFO

Article history:
Received 23 March 2015
Received in revised form
16 September 2015
Accepted 17 September 2015

Keywords:
Rehabilitation robotics
Active orthosis
Series Elastic Actuator
Robust torque control
Impedance control

ABSTRACT

Active orthosis is one of the main research topics in the field of motor recovery. This paper deals with the design and control of an active knee orthosis driven by a customized rotary Series Elastic Actuator (SEA). The proposed actuator includes a DC motor, a worm gear and a customized torsion spring. Since the elastic element is the most important component in SEA design, a finite element analysis of the spring is performed to meet the specific requirements for knee assistance. Torque and impedance control are implemented to ensure secure interaction with the patient and to enable new strategies for rehabilitation. The torque controller, cascaded with an inner motor velocity control loop, is based on $\mathcal{H}_\infty$ criterion to achieve good system performance with relation to parametric uncertainties and external disturbances. The impedance control is implemented using a PD position controller in cascade with the torque controller, where the outer position controller determines the desired torque according to position and velocity errors and impedance parameters. A variable impedance control strategy is then implemented to show the possibility to regulate the impedance of the knee joint during walking. Experiments considering the interaction between the subject and the active orthosis are performed to evaluate the proposed controllers.

1. Introduction

The use of robotic devices for rehabilitation of neurological patients is increasing rapidly due to the importance of functional exercises that stimulate motor cortex and promote motor recovery (Ferris, Sawicki, & Domingo, 2006). Studies suggest that rehabilitation of post-stroke patients was intensified with robot-assisted therapy (Kwakkel, Kollen, & Krebs, 2008; Prange, Jannink, Groothuis-Oudshoorn, Hermens, & Ijzerman, 2006). The advantages of robotic therapy compared with traditional ones also include the ability to evaluate patient progress constantly through objective measures, and the possibility of customizing the treatment according to the patient's level of commitment.

In general, robotic therapy includes a combination of exercises involving passive, active-assisted or active-resisted movements. This combination of exercises can be obtained through the use of impedance control, proposed by Hogan (1985), which allows to configure the dynamic interaction between the device and the patient. For example, an active orthosis can provide support torque during gait training in a assist-as-needed basis. During remaining part of the gait, the orthosis need to present a low impedance behavior, so as to be fully compliant with the patient's actions. The impedance control can also be used to impose a controlled resistance to the patient movement aiming to strengthen muscle groups.

To effectively assist human motion and, at the same time, guarantee patient safety, rehabilitation robots must satisfy certain requirements such as precise and large torque generation, with a bandwidth that approximates muscle movement. It is also essential to ensure a backdrivable behavior, characterized by a low mechanical impedance. Traditional stiff and high-precision actuators do not meet these critical requirements (Ham, Sugar, Vanderborght, Hollander, & Lefeber, 2009; Santis, Siciliano, Luca, & Bicchi, 2008). A simple and effective solution, initially proposed in Pratt and Williamson (1995), is the Series Elastic Actuator (SEA) concept, where elasticity is intentionally introduced in series between a gear-motor and the load. This configuration allows decoupling the gear-motor inertia and other nonlinearities from the

☆This work was supported by São Paulo Research Foundation (FAPESP) under Grants 2011/04074-3 and 2013/14756-0. An earlier version of this paper was presented at the 19th World Congress of the International Federation of Automatic Control (IFAC 2014).

* Corresponding author at: Department of Mechanical Engineering, Engineering School of São Carlos, University of São Paulo, 13566-590 São Carlos, Brazil. Fax: +55 1633739402.
E-mail addresses: wilianmds@sc.usp.br (W.M. dos Santos), gcaurin@sc.usp.br (G.A.P. Caurin), siqueira@sc.usp.br (A.A.G. Siqueira).

http://dx.doi.org/10.1016/j.conengprac.2015.09.008
0967-0661/

output and isolates the drivetrain from shocks introduced by the load. Another important feature is that the elastic element can be used as a torque sensor considering the linear relationship between spring deflection and torque.

A rotary SEA to assist the movement of lower limbs was presented in Kong, Bae, and Tomizuka (2009). It consists of a geared DC motor, a helical torsion spring and two rotary potentiometers used to detect the position of the output shaft and the deformation of the spring. In the proposed configuration, the spring is directly placed between the gear-motor and the human joint, therefore subjected to large torques. Helical torsion springs able to support large torques are usually stiff for the considered application. Stiff springs are less sensitive to small torques, resulting in lower torque control accuracy. Moreover, their nonlinearities are not negligible. The spring constant values for gait assistance usually lie in the range from 100 to 300 N m/rad (Carpino, Accoto, Sergi, Tagliamonte, & Guglielmelli, 2012), with the maximum torque in the range from 10 to 100 N m (Kong, Bae, & Tomizuka, 2012; Lagoda, Schouten, Stienen, Hekman, & van der Kooij, 2010; Sergi, Accoto, Carpino, Tagliamonte, & Guglielmelli, 2012; Stienen et al., 2010).

From these considerations, a new rotary SEA model was proposed by the same authors in Kong et al. (2012). In this new configuration, the spring is inserted between the worm gear and the output gears, thereby enabling the use of a spring with low stiffness. The disadvantage of this configuration is that the nonlinearities associated with the output gears compromise the fidelity of measured torque, increasing the uncertainties in the system.

A solution adopted by some researchers is to propose an arrangement of linear springs so as to obtain a torsion elastic element (Tsagarakis, Laffranchi, Vanderborght, & Caldwell, 2009; Yoon et al., 2005). This approach allows the insertion of elastic elements with low stiffness directly between the gear-motor and the load. However, a linear behavior in the torque versus angle relationship is difficult to be obtained. Another solution is the development of customized elastic element (Carpino et al., 2012; Lagoda et al., 2010). In addition to allowing the elastic element to be connected to the load in a direct-drive configuration, this approach may reduce some problems such as residual deflection, hysteresis and a non-linear behavior in the torque versus angle relationship that negatively affect accurate torque estimation and consequently control performance.

Considering these concepts, a new customized torsion spring configuration for rotary SEA is proposed in this paper. The torsion spring design was optimized using Finite Element Method (FEM) simulations in order to satisfy the specific requirements to partially support the knee joint flexion/extension during physical therapy in individuals with low motor impairment. The value 15 N m, which corresponds to 60% of the peak torque from the gait pattern, is defined as design requirement for the maximum torque of the actuator. Robust $\mathcal{H}_\infty$ torque and impedance controllers are designed to ensure secure interaction with the patient and good system performance. The performance of the controllers is evaluated by frequency response analysis, where it can be verified that a suitable bandwidth was achieved. Experimental results obtained from the implementation of a variable impedance control strategy during walking are presented. The design of $\mathcal{H}_\infty$ controllers for robot-aided rehabilitation and their performance; as well as the design of the customized torsion spring are the main contributions of this paper.

This paper is organized as follows: Section 2 describes the design requirements; Section 3 presents in detail the mechanical design of the rotary SEA; Section 4 presents the torque and impedance controllers design; Section 5 presents the experimental results obtained from the active knee orthosis; Section 6 presents the conclusions.

2. Design requirements

The design requirements are based on body mass normalized data described in Kirtley (2006) for gait cycles. Considering that the maximum power exerted by the knee joint is 0.739 W/kg, with a maximum torque of 0.365 N m/kg, and that the active knee orthosis should be able to supply 60% of the peak torque from the gait pattern of a healthy person with approximately 70 kg, the new robotic device must provide a torque assistance up to 15 N m. The minimum torque bandwidth is determined by the Power Spectral Density (PSD) of knee joint torque. Regarding that more than 95% of the PSD of knee joint torque is in the frequency range between 0 and 5 Hz a minimum bandwidth of 5 Hz is defined as a requirement to torque control.

The elastic element must be carefully designed, since it is the most important component in the SEA. The spring constant is defined through selection procedures described in Robinson (2000). Basically, they define lower and upper bounds for spring constant based on desired large torque bandwidth and low output impedance, respectively. First, consider the simplified model of Fig. 1 which includes the equivalent inertia, J_{eq}, and damping, B_{eq}. At this point, these values consider only the inertia and damping of the motor seen through the transmission (the complete values of J_{eq} and B_{eq} are defined in (10) and (11), respectively). The torque applied to the load at the frequency domain, $\tau_l(s)$, is found as

$$\tau_l(s) = \frac{k_s}{J_{eq}s^2 + B_{eq}s + k_s}\tau_m(s) - \frac{k_s(J_{eq}s^2 + B_{eq}s)}{J_{eq}s^2 + B_{eq}s + k_s}\theta_l(s), \tag{1}$$

where τ_m is the torque generated by the motor, θ_l is the load position, and k_s is the spring constant.

The ability of the actuator to produce large torques is limited in frequency by the maximum torque which the motor can generate. To define the large torque bandwidth, the load position is considered fixed and the torque from the motor is set to its maximum value τ_{max} (maximum continuous torque from motor datasheet). Hence, the transfer function from τ_{max} to the maximum output torque, $\tau_{l_{max}}$, is given by

$$\frac{\tau_{l_{max}}(s)}{\tau_{max}(s)} = \frac{k_s}{J_{eq}s^2 + B_{eq}s + k_s}. \tag{2}$$

The saturation frequency, i.e., the frequency at which the above system begin to fall off, is defined from (2) as

$$\omega_0 = \sqrt{\frac{k_s}{J_{eq}}}. \tag{3}$$

Therefore, the higher the spring constant, the greater the large torque bandwidth. Eq. (3) is used to define the lower bound for the spring constant. Fig. 2(a) shows the frequency responses for (2) considering three values of spring constant (100 N m/rad, 200 N m/rad, and 300 N m/rad) and the parameters of the selected motor.

To analyze the output impedance, a simple proportional controller is defined ($\tau_m = K_p(\tau_d - \tau_l)$). Assuming a constant desired output torque ($\tau_d = \tau_0$), the output impedance is given by

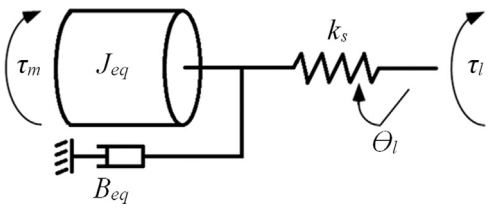

Fig. 1. Schematic of rotary Series Elastic Actuator.

Please cite this article as: dos Santos, W. M., et al. Design and control of an active knee orthosis driven by a rotary Series Elastic Actuator. *Control Engineering Practice* (2015), http://dx.doi.org/10.1016/j.conengprac.2015.09.008

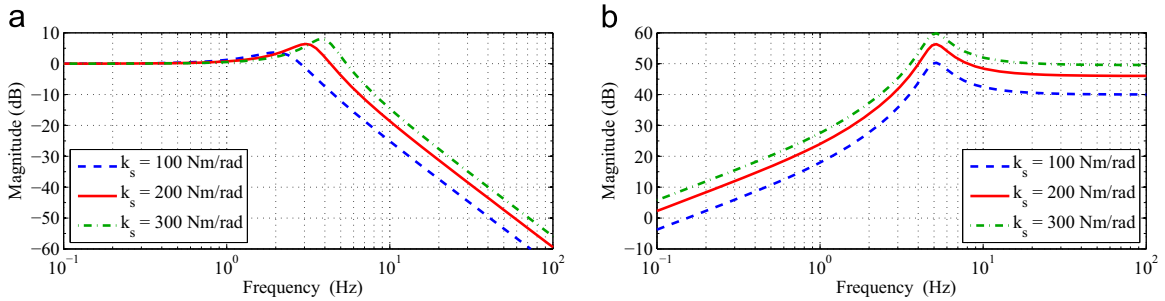

Fig. 2. The closed-loop large torque bandwidth and actuator output impedance. (a) Bode plot for large torque transfer function. (b) Bode plot for impedance transfer function.

$$\frac{\tau_l(s)}{\theta_l(s)} = -\frac{k_s(J_{eq}s^2 + B_{eq}s)}{J_{eq}s^2 + B_{eq}s + k_s(1 + K_p)}. \quad (4)$$

Fig. 2 (b) shows the frequency responses for (4). The controller gain K_p is defined so that the controlled natural frequency, $\omega_c = \sqrt{k_s(1 + K_P)/J_{eq}}$, results in 5 Hz, the minimal desired closed loop bandwidth. Note that decreasing k_s linearly lowers the impedance profile. Also, at high frequencies, the output impedance converges to the spring constant. Considering this result, a spring constant of 200 N m/rad is defined as target value for the design. It results in a large torque bandwidth of $\omega_0 = 3.3$ Hz and a near 0 dB output impedance for low frequencies.

Finally, the actuator must be as compact and lightweight as possible. Therefore, it is specified a maximum weight of 2.5 kg.

3. Mechanical design

The mechanical design was conceived in order to obtain a compact and lightweight architecture. All housing parts are made of aluminum for the purpose of reducing weight. The final assembly of the rotary SEA consists of: (a) Maxon Motor RE 40, graphite brushes, 150 W DC motor; (b) worm gear set (M1-150 of HPC Gears International Ltd.) with reduction ratio of 150:1; (c) customized torsion spring; (d) angular contact bearings; (e) magneto-resistant incremental encoder; and (f) opto-electronic incremental encoder. The overall dimensions are shown in Fig. 3 and the resulting mass is 2.53 kg, allowing direct mounting of the actuator on the frame of a knee orthosis.

The choice of gear-motor was made based on the characteristics of the knee joint considering gait pattern of a healthy person. The angular velocities of the knee joint are in the range of ± 50 rpm and the maximum torque required for the project is 15 N m (see Section 2), while the maximum continuous torque and the maximum velocity of the selected motor are respectively

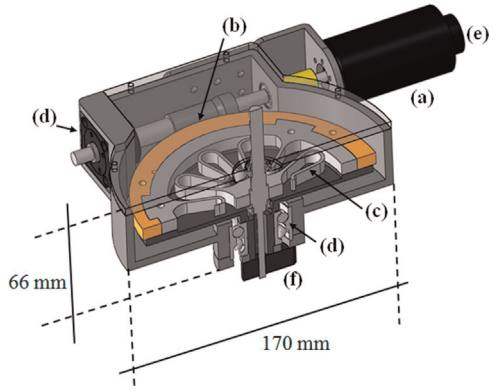

Fig. 3. Cross section of the rotary SEA showing drivetrain components.

0.181 N m and 8200 rpm. Therefore a worm gear set with reduction ratio of 150:1 is used to adjust the operating range of motor in order to fulfill the requirements for velocity and torque. Thereby, the worm gear output can operate in a velocity range of ± 55 rpm and, if the efficiency of the gears is not considered, it can provide a maximum continuous torque of 27.15 N m. However, the friction between the gear reduces significantly the efficiency and the torque amplification ratio is not necessarily the same as the ratio velocity reduction (Kong et al., 2012). For this reason, a safety factor of 1.8 to the torque requirement is considered.

All relevant information to the control system, i.e. motor rotation, actuator output, and spring deflection estimate, are obtained by two encoders. A magneto-resistant incremental encoder Maxon with a resolution of 4096 pulses per revolution in quadrature decoding mode is used to measure the motor rotation and allows estimation of the position of the worm wheel. An opto-electronic incremental encoder Maxon HEDS 5540 with a resolution of 2000 pulses per revolution in quadrature decoding mode is used to measure the actuator output. The spring deflection estimate is obtained by the difference between the position of the worm wheel and the actuator output. The theoretical output torque resolution, bounded by the lower output encoder resolution, is given by $k_s(2\pi/2000)$, where k_s is the spring constant.

3.1. Customized torsion spring

To meet the requirements of the proposed application, the elastic element must be compact, lightweight, and able to withstand high torque with low intrinsic stiffness. However, these characteristics are not found in torsion springs usually available. For this reason, a new topology torsion spring is proposed. Fig. 4 (a) shows a schematic perspective view of the customized torsion spring. It is composed of two rings interconnected by flexible elements defined by finite element analysis. The material selected for analysis and manufacture was chromium–vanadium steel (AISI 6150), with Young's modulus of 205 GPa and a yield strength of approximately 1320 MPa after a heat treatment process. Although there are other steels with better characteristics for such application, the AISI 6150 is considered in this work because it is an inexpensive steel and can be easily found in the market.

The stress distribution and deformation of the customized spring was analyzed by the FEM, using ANSYS® software to ensure that the maximum stress is less than the yield strength of the material when subjected to the maximum torque. The analysis consists in fixing the inner ring of the spring while tangential forces equivalent to the input torque are applied on the outer ring. The theoretical spring stiffness is computed by the ratio between the torque applied and the corresponding angular deformation obtained in the simulation. In the first analysis, it was observed that the stress concentration is located in the inner corner radius, R_4, Fig. 4(b).

In order to find the lowest stress value for a given stiffness, the

Please cite this article as: dos Santos, W. M., et al. Design and control of an active knee orthosis driven by a rotary Series Elastic Actuator. *Control Engineering Practice* (2015), http://dx.doi.org/10.1016/j.conengprac.2015.09.008

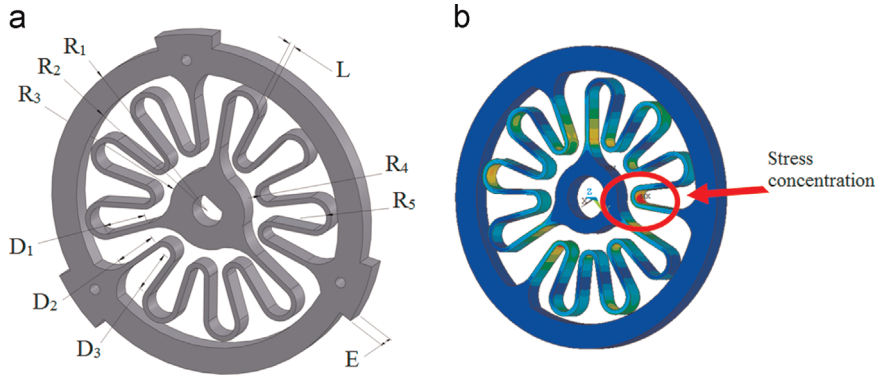

Fig. 4. Customized torsion spring design. (a) Schematic perspective view of the torsion spring. (b) Static simulation for stress distribution.

following methodology was adopted. The value of radius R_4 was varied from 2.5 to 3.5 mm with a step of 0.05 mm for each thickness (E) from 5 to 8 mm with a step of 0.5 mm. The values of D_1, D_2 and D_3 were varied proportionally to the R_4 whereas the values of R_1, R_2, R_3, R_5 and L were kept constant in order to not change the proposed topology. Fig. 5 shows the results of the adopted methodology. From Fig. 5(a) a linear approximation can be used to characterize the directly proportional relationship between spring geometry parameters (R_4 and E) and spring constant. When Fig. 5 (b) is analyzed, a similar behavior is observed between geometric parameter R_4 and von Mises stress, however, in an inversely proportional way. It can also be observed that the inversely proportional relationship between geometry parameter E and Von Mises stress is characterized by a non-linear behavior. It is observed in Fig. 5(b) that the distances between the curves are decreasing as the thickness increases.

The values obtained in the simulation for the geometry parameters R_4 and E that had lower stress for the desired stiffness of 200 N m/rad are respectively 2.8 and 8 mm. In order to evaluate the proposed topology, two other springs with thickness (E) of 6 and 7 mm, corresponding to the spring constant (theoretical) of 150 and 175 N m/rad, were manufactured. The other parameters are shown in Table 1.

The maximum values of von Mises stress obtained in the simulation were 732, 622 and 541 MPa for each spring with thickness (E) of 6, 7 and 8 mm, respectively. Thus a safety factor of 1.8 from the highest value of stress is considered. The customized torsion spring, shown in Fig. 6(a), has been manufactured using the Wire Electrical Discharge Machining (WEDM) process. Fig. 6 (b) shows the final assembly of the rotary SEA.

Experimental characterization of the spring stiffness was performed by coupling on the output shaft of the rotary SEA in a torque sensor (Gamma SI-65-5 from ATI Industrial Automation, Inc.). The rotary SEA was programmed to follow a position profile consisting of a sequence of steps (amplitude 0.14°, duration 10 s) in both loading and unloading conditions, while the torque was measured by the sensor. Fig. 7 shows the obtained results.

Table 1
Customized torsion spring geometry parameters (mm).

E	L	D_1	D_2	D_3	R_1	R_2	R_3	R_4	R_5
6, 7 & 8	2	17.6	17	17.1	62.5	52.5	15	2.8	5.3

A linear regression was performed in both directions (compression and extension). From the obtained results it is possible to observe a backlash with amplitude of ± 0.0044 rad occasioned by intrinsic feature of the worm gear set. In order to compensate the backlash on the sensor measurement, two lines are defined connecting the origin to the regression lines at the points corresponding to ± 0.01 rad of deflection, as illustrated in Fig. 7(d). With this compensation, it is possible to estimate low torques applied to the load. An initial positioning procedure is used to align the motor shaft to the center of the backlash. The output shaft is positioned with its longitudinal axis perpendicular to the horizontal plane. The motor is set to move slowly in one direction until the output encoder measures one pulse. From this point, the same procedure is done in the opposite direction. The difference between the measures of the motor position at the extreme points is an estimate of the backlash amplitude.

The corresponding values of the spring constant (k_s) are shown in Table 2. Note that when the spring is compressed (positive deflection), the stiffness is larger than when it is extended (negative deflection). The value of the spring constant determined experimentally is approximately 50% lower than the obtained by finite element analysis. This discrepancy is probably due to the properties of the material being different from the nominal used in the simulation and the imperfections in the model and mesh used in the analysis. The assembly of the orthosis with the rotary SEA attached to it is shown in Fig. 8.

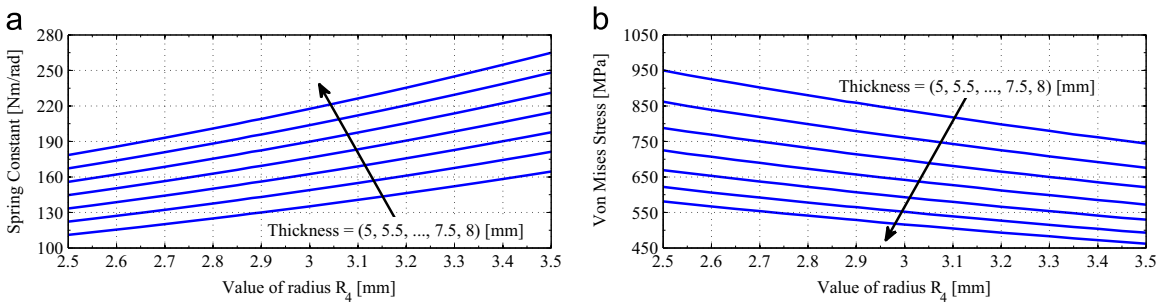

Fig. 5. Results of the methodology adopted. The arrows indicate the direction of increasing spring thickness. (a) Geometry parameters vs. spring constant. (b) Geometry parameters vs. von Mises stress.

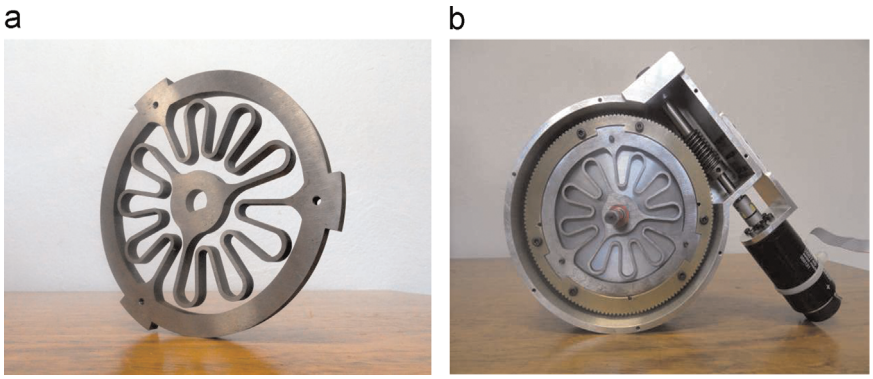

Fig. 6. Customized spring and rotary Series Elastic Actuator. (a) Customized torsion spring. (b) Rotary SEA.

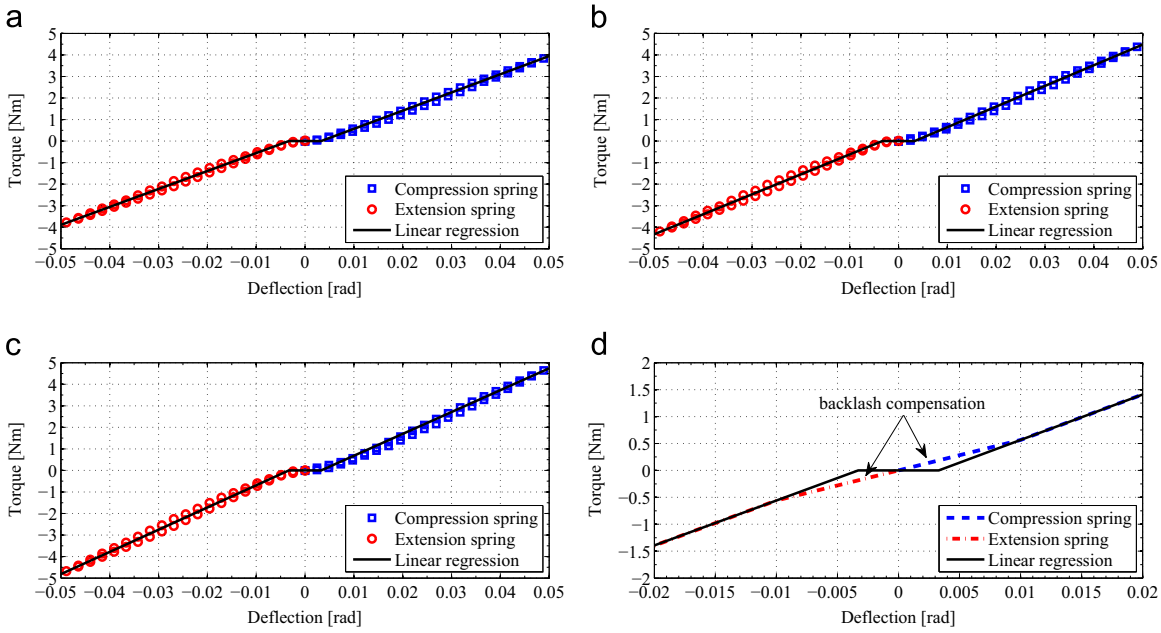

Fig. 7. Characterization of the customized torsion spring. (a) Spring 1 – thickness of 6 mm and stiffness equal to 84 N m/rad. (b) Spring 2 – thickness of 7 mm and stiffness equal to 94 N m/rad. (c) Spring 3 – thickness of 8 mm and stiffness equal to 105 N m/rad. (d) Spring 1 – backlash compensation on the sensor measurement.

Table 2
Customized torsion spring physical parameters.

Spring	Mass (kg)	k_s simulated (N m/rad)	k_s real (N m/rad)	
			Extension	Compression
1	0.292	150	82	85
2	0.338	175	92	96
3	0.384	200	103	106

Fig. 8. Rotary SEA attached to a knee orthosis.

Please cite this article as: dos Santos, W. M., et al. Design and control of an active knee orthosis driven by a rotary Series Elastic Actuator. *Control Engineering Practice* (2015), http://dx.doi.org/10.1016/j.conengprac.2015.09.008

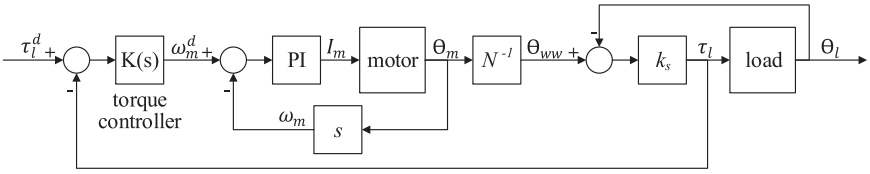

Fig. 9. Block diagram of the torque control with inner velocity loop.

4. Controller design

4.1. Control hardware

The control hardware consists of a EPOS 24/5 Positioning Controller, Maxon Motor, and an ordinary computer hardware equipped with a CAN communication card sold by National Instruments. The EPOS is a full digital smart motion controller capable of operating in position, velocity and current modes. The device is also responsible to decode the signals from quadrature encoders. The communication interface between the computer hardware and the EPOS is performed by CANopen communication protocol. The frequency of the control loop is set to 200 Hz.

In adopted approaches traditionally for SEA torque control, the motor is treated as a torque source. This assumption is justified since the current applied to the motor is directly proportional to the output torque. However, this approach becomes difficult to implement due to the intrinsic nonlinearities of the drivetrain such as backlash, stiction, and efficiency losses. In Robinson (2000), it is suggested to treat the motor as a velocity source rather than as a torque source. According to Wyeth (2006), this approach helps to overcome these undesirable effects of the gear-motor.

The block diagram of the torque control loop is illustrated in Fig. 9. The inner velocity loop is performed by the built-in EPOS velocity control. The PI controller parameters were defined by the automatic tunning procedure available in the device configuration set-up.

The torque applied to the load is calculated as $\tau_l = k_s(\theta_{ww} - \theta_l)$, where θ_l is the load position and θ_{ww} is the worm wheel position given by $\theta_{ww} = \theta_m N^{-1}$, where θ_m is the motor position and N^{-1} is the reduction ratio. It is filtered through a second-order low-pass Butterworth filter with a cut-off frequency of 50 Hz.

4.2. Dynamic model

The transfer function of the rotary SEA can be obtained as described in the sequence. Regarding Fig. 10, the input torque (τ_{in}) can be expressed by

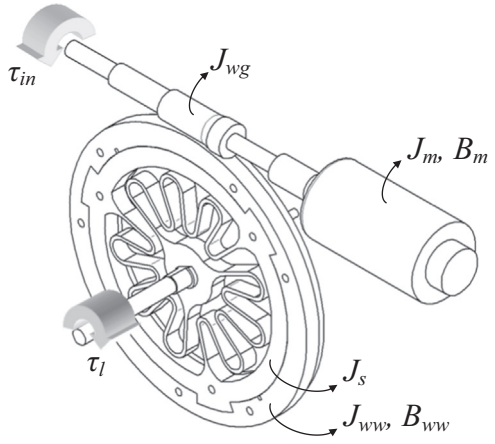

Fig. 10. Dynamic model of the rotary SEA.

$$\tau_{in}(s) = \tau_m(s) - (J_m + J_{wg})\theta_m(s)s^2 - B_m\theta_m(s)s, \tag{5}$$

where τ_m represents the torque generated by the motor, J_m and J_{wg} are the rotational inertias of the motor and the worm gear, respectively, and B_m is the damping coefficient of the motor.

Similarly, the output torque (τ_{out}) can be written as

$$\tau_{out}(s) = (J_s + J_{ww})\theta_{ww}(s)s^2 + B_{ww}\theta_{ww}(s)s + \tau_l(s), \tag{6}$$

where J_s and J_{ww} are, respectively, the rotational inertias of the spring and worm wheel, B_{ww} is the damping coefficient of the drivetrain, and τ_l is the torque applied to the load.

Since the torque generated by the motor is amplified by the velocity reduction ratio, the following kinematic conditions can be considered:

$$\tau_{out}(s) = N\tau_{in}(s) \tag{7}$$

and

$$\theta_{ww}(s) = N^{(-1)}\theta_m(s), \tag{8}$$

where $N^{(-1)}$ is the reduction ratio.

Substituting (5) and (6) into (7), and (8) into the resulting equation, one obtains

$$J_{eq}\theta_{ww}(s)s^2 + B_{eq}\theta_{ww}(s)s = N\tau_m(s) - \tau_l(s), \tag{9}$$

where J_{eq} is the equivalent rotational inertia and B_{eq} is the equivalent damping coefficient, defined as

$$J_{eq} = J_{ww} + J_s + (J_m + J_{wg})N^2 \tag{10}$$

and

$$B_{eq} = B_{ww} + B_m N^2. \tag{11}$$

As in the adopted approach the motor is treated as a velocity source and considering that the desired current is equal to the actual current, the motor torque can be computed as

$$\tau_m(s) = k_t\left[\left(k_p + \frac{k_i}{s}\right)\omega_m^d(s) - \left(k_p + \frac{k_i}{s}\right)\omega_m(s)\right], \tag{12}$$

where k_p and k_i are the proportional and integral gains of the velocity controller, respectively, k_t is the motor torque constant, ω_m^d is the desired motor velocity, and ω_m is the motor velocity, which can be expressed by $\omega_m(s) = N\theta_{ww}(s)s$.

Substituting (12) into (9) and rewriting $\theta_{ww}(s)$ as $\tau_l(s)/k_s + \theta_l(s)$, one gets the open-loop transfer function of the system as a function of two variables ω_m^d and θ_l as

$$\tau_l(s) = \frac{\left(\frac{Nk_sk_tk_p}{J_{eq}}\right)s + \left(\frac{Nk_sk_tk_i}{J_{eq}}\right)}{s^3 + \left(\frac{B_{eq} + k_tk_pN^2}{J_{eq}}\right)s^2 + \left(\frac{k_s + k_tk_iN^2}{J_{eq}}\right)s}\omega_m^d(s) - \frac{k_ss^2 + \left(\frac{B_{eq}k_s + N^2k_sk_tk_p}{J_{eq}}\right)s + \left(\frac{N^2k_sk_tk_i}{J_{eq}}\right)}{s^2 + \left(\frac{B_{eq} + k_tk_pN^2}{J_{eq}}\right)s + \left(\frac{k_s + k_tk_iN^2}{J_{eq}}\right)}\theta_l(s). \tag{13}$$

Please cite this article as: dos Santos, W. M., et al. Design and control of an active knee orthosis driven by a rotary Series Elastic Actuator. *Control Engineering Practice* (2015), http://dx.doi.org/10.1016/j.conengprac.2015.09.008

Table 3
Rotary SEA model parameters.

k_s (N m/rad)	J_{eq} (kg m^2)	B_{eq} (N m s/rad)	k_t (A/N m)	N	k_p (N m s/rad)	k_i (N m/rad)
84, 94 & 105	0.47	60	0.03	150	11.9	1.19

However, for the controller design it was considered the case where the load is fixed ($\theta_l=0$). Therefore, open-loop transfer function of the system is given by

$$G(s)=\frac{\tau_l(s)}{\omega_m^d(s)}=\frac{\left(\frac{Nk_sk_tk_p}{J_{eq}}\right)s+\left(\frac{Nk_sk_tk_i}{J_{eq}}\right)}{s^3+\left(\frac{B_{eq}+k_tk_pN^2}{J_{eq}}\right)s^2+\left(\frac{k_s+k_tk_iN^2}{J_{eq}}\right)s}, \tag{14}$$

where the parameters are defined in Table 3. Although the equivalent rotational inertia, J_{eq}, depends on the spring rotational inertia, J_s, its value has not changed since the difference between the rotational inertia of the springs is small and the predominant term in (10) is defined by the high reduction ratio N.

4.3. $\mathcal{H}_\infty$ torque control

This section presents the linear $\mathcal{H}_\infty$ control design and the procedures to apply it for torque control of rotary SEA. It adopts the mixed-sensitivity $\mathcal{H}_\infty$ control procedure over the sensitivity ($S(s)$) and the control sensitivity ($K(s)S(s)$) transfer functions, as presented in Skogestad and Postlethwaite (2005), where $S(s)=(I+G(s)K(s))^{-1}$ and $K(s)$ is the resulting controller. It ensures robust tracking performance, disturbance rejection, and defines the size and bandwidth of the controller (to limit the control energy), with relation to the worst-case bounded ($\mathcal{L}_2$) external inputs acting on the system (robustness with relation to uncertainties is not guaranteed). The procedure consists in defining functions $W_e(s)$ and $W_u(s)$ to weight $S(s)$ and $KS(s)$, respectively.

The transfer function $W_e(s)$ is defined as

$$W_e(s)=\frac{1}{M_s}\frac{s+\omega_s}{(s+\omega_s\epsilon_s)}, \tag{15}$$

where ω_s is the closed-loop bandwidth, M_s is the maximum peak for the sensitivity function, and $\epsilon_s>0$ is the maximum steady-state error. M_s defines the maximum amplification of high frequency noises and the limits for the overshoot. The transfer function $W_u(s)$ is defined as

$$W_u(s)=\frac{1}{M_u}\frac{s+\omega_u}{\left(s+\frac{\omega_u}{\epsilon_u}\right)}, \tag{16}$$

where ω_u is the controller bandwidth, M_u is the maximum controller gain for high frequencies, and $\epsilon_u>0$ is a small value set to ensure that the cost function is dominated by $W_e(s)$ at low frequency, and to guarantee that the controller design is well-posed. The weighting functions' parameters are shown in Table 4.

Fig. 11 shows the block diagram of the SEA torque control represented in $\mathcal{H}_\infty$ control framework. It considers the weighting functions $W_e(s)$ and $W_u(s)$ which scale the error (e) and the input (u), respectively. The parametric uncertainties and external disturbances acting on the plant output are grouped in the combined disturbance $d(t)$.

Table 4
Weighting functions parameters.

M_s (dB)	ω_b (rad/s)	ε	M_u (dB)	ω_{bc} (rad/s)	ε_1
29	600	0.0012	44	600	0.01

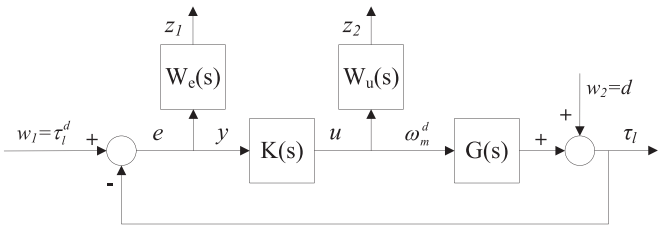

Fig. 11. Block diagram of the $\mathcal{H}_\infty$ torque control.

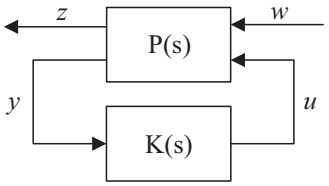

Fig. 12. Block diagram for $\mathcal{H}_\infty$ control.

$\mathcal{H}_\infty$ control framework considers the system block diagram as shown in Fig. 12, where $P(s)$ represents the augmented plant (nominal plant $G(s)$ plus weighting functions) and $K(s)$ the controller. The plant has two sets of input signals, the internal input u and the external input $\mathbf{w}$, and two sets of output signals, the measured signal y and the regulated output $\mathbf{z}$. Regarding Fig. 11:

$$u=\omega_m^d,\quad \mathbf{w}=\begin{bmatrix}w_1\\w_2\end{bmatrix}=\begin{bmatrix}\tau_l^d\\d\end{bmatrix},$$

$$y=e,\quad \mathbf{z}=\begin{bmatrix}z_1\\z_2\end{bmatrix}=\begin{bmatrix}W_e e\\W_u u\end{bmatrix}.$$

The objective of $\mathcal{H}_\infty$ controllers is to guarantee that $\mathcal{H}_\infty$ norm of the transfer function from input $\mathbf{w}$ to output $\mathbf{z}$, $\mathbf{T_{zw}}(s)$, be bounded by an attenuation level γ. Regarding the mixed-sensitivity $\mathcal{H}_\infty$ control, this condition is given by

$$\|\mathbf{T_{zw}}(s)\|_\infty=\left\|\begin{matrix}\mathbf{W_e}(s)\\\mathbf{W_u}(s)\end{matrix}\right\|_\infty\le\gamma,$$

where $\mathbf{W_e}(s)=[W_e(s)S(s)\ \ -W_e(s)S(s)]$ and $\mathbf{W_u}(s)=[W_u(s)K(s)S(s)-W_u(s)K(s)S(s)]$. The parameter γ indicates the level of robustness of the control system with relation to the worst-case bounded disturbance $\mathbf{w}$. The resulting values of $S(s)$ and $K(s)S(s)$ satisfy the following inequalities:

$$\bar{\sigma}(S(j\omega))\le\gamma\underline{\sigma}(W_e^{-1}(j\omega)),$$

and

$$\bar{\sigma}(K(j\omega)S(j\omega))\le\gamma\underline{\sigma}(W_u^{-1}(j\omega)),$$

where $\bar{\sigma}(H(j\omega))$ and $\underline{\sigma}(H(j\omega))$ are the greatest and least singular values of the transfer function $H(s)$ over the frequency ω, respectively. Fig. 13 shows the graphics of the sensitivity function $S(j\omega)$ versus the weighting function $\gamma W_e^{-1}(j\omega)$, and of $K(j\omega)S(j\omega)$ versus $\gamma W_u^{-1}(j\omega)$, for the resulting controller $K_1(j\omega)$. Note that the controlled plant curves are lower than the weighting functions for all frequency. The level of attenuation γ for this case is 0.137.

4.3.1. Torque control bandwidth

Torque control bandwidth was determined through Frequency Response Function (FRF) analysis, obtained from $H_1(j\omega)$ and $H_2(j\omega)$

Please cite this article as: dos Santos, W. M., et al. Design and control of an active knee orthosis driven by a rotary Series Elastic Actuator. *Control Engineering Practice* (2015), http://dx.doi.org/10.1016/j.conengprac.2015.09.008

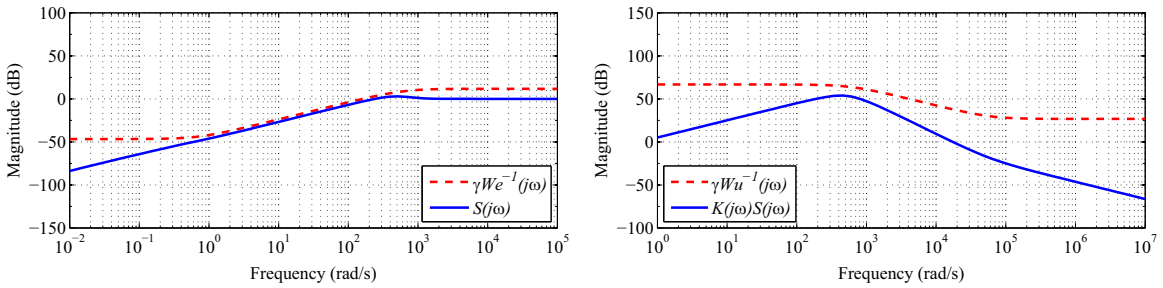

Fig. 13. Sensitivity function $S(j\omega)$ vs. $\gamma W_e^{-1}(j\omega)$ and $K(j\omega)S(j\omega)$ vs. $\gamma W_u^{-1}(j\omega)$.

estimators as proposed in Maia and Silva (1997). The estimator $H_1(j\omega)$ considers the presence of random noise in the output signal, and in this case, the FRF is calculated as $H_1(j\omega) = S_{XY}(j\omega)/S_{XX}(j\omega)$, where $S_{XY}(j\omega)$ is the cross-spectrum of the input and output signal, and $S_{XX}(j\omega)$ is the auto-spectrum of the input signal; the estimator $H_2(j\omega)$ considers the presence of random noise in the input signal, and in this case, the FRF is calculated as $H_2(j\omega) = S_{YY}(j\omega)/S_{XY}(j\omega)$, where $S_{YY}(j\omega)$ is the auto-spectrum of the output signal. The results obtained by the estimators can be evaluated through the ordinary coherence function $C(j\omega)$, defined as the ratio of the $H_1(j\omega)$ estimator over the $H_2(j\omega)$ estimator. The ordinary coherence function is always a real value between 0 and 1, where a value near to 1 represents a good estimate of both estimators.

To implement the estimation method, the desired torque (τ_l^d), seen here as an input signal, was defined as a chirp signal with amplitude of 5 N m and frequency varying from 0 to 20 Hz and back to 0 Hz in 20 s. The signal is repeated four times, totaling a sampling period of 80 s. Fig. 14 shows the Bode plot of the closed loop transfer function computed from $H_1(j\omega)$ and $H_2(j\omega)$ estimators and the coherence function $C(j\omega)$ for the rotary SEA assembled with springs 1 and 3. The values of the torque control bandwidth for the proposed SEA assembled with springs 1, 2 and 3 are respectively 6.8, 8.5 and 9.6 Hz. Note that there is a directly proportional relationship between spring stiffness and torque control bandwidth. This is consistent with the literature, e.g. Robinson, Pratt, Paluska, and Pratt (1999).

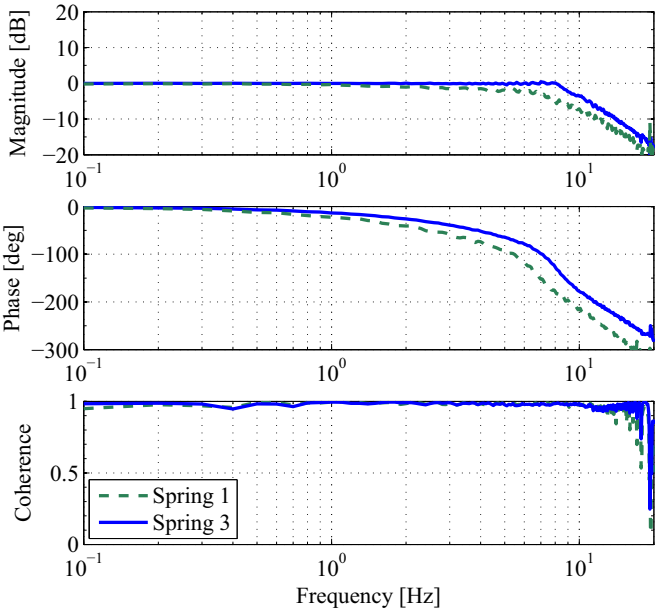

Fig. 14. Frequency response of the torque control.

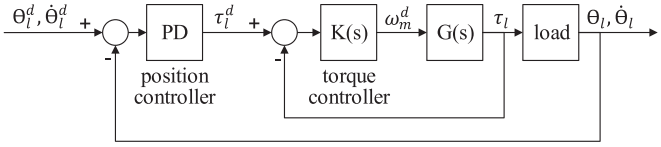

Fig. 15. Block diagram of the impedance control with inner loop $\mathcal{H}_\infty$ torque control.

4.4. Impedance control

The impedance control is implemented through a PD position controller in cascade with $\mathcal{H}_\infty$ torque controller. This approach is similar to that proposed in Santos and Siqueira (2014), however, this paper includes an inner robust controller. Fig. 15 shows the block diagram of the proposed control scheme. The outer position controller determines the desired torque (τ_l^d) according to position and velocity errors and impedance parameters. Thus, the desired torque can be expressed by

$$\tau_l^d = k_v(\theta_l^d - \theta_l) + b_v(\dot{\theta}_l^d - \dot{\theta}_l), \tag{17}$$

where k_v and b_v are the virtual stiffness and damping, respectively.

Two experiments were conducted in order to evaluate the ability of rotary SEA to reproduce the behavior of the knee joint impedance within a frequency range suitable for the given application. First, considering a pure damping control through transfer function $T_b(j\omega) = \tau_l(j\omega)/\dot{\theta}_l(j\omega)$. In the second experiment, considering a pure stiffness control through transfer function $T_k(j\omega) = \tau_l(j\omega)/\theta_l(j\omega)$. The input signals used to estimate the FRF in both experiments were generated by a human operator by imposing oscillating movements to the SEA output shaft.

4.4.1. Damping control

The pure damping control was obtained by setting $\theta_l^d = 0$ and $k_v = 0$, and evaluated varying the value of b_v in 5, 10 and 15 N m s/rad, for the rotary SEA assembled with the different springs. Fig. 16 shows the Bode plot of the closed loop transfer function $T_b(j\omega)$, computed from $H_1(j\omega)$ and $H_2(j\omega)$ estimators, and the coherence function between them, considering the SEA assembled with Spring 3. The damping control bandwidth is approximately 3 Hz and no significant variations in bandwidth were observed for the different values of b_v and different values of spring constant. However, a difference of 3 N m s/rad was evidenced between the desired value of b_v and the actual value, demonstrating the existence of an intrinsic damping in the system.

4.4.2. Stiffness control

Similar to the first experiment, pure stiffness control was also evaluated by setting $\theta_l^d = 0$ and $b_v = 0$, and varying the value of k_v in 10, 30 and 60 N m/rad, for the rotary SEA assembled with the different springs. Fig. 17(a) shows the Bode plot of the closed loop transfer function $T_k(j\omega)$ and the coherence function, considering

Please cite this article as: dos Santos, W. M., et al. Design and control of an active knee orthosis driven by a rotary Series Elastic Actuator. *Control Engineering Practice* (2015), http://dx.doi.org/10.1016/j.conengprac.2015.09.008

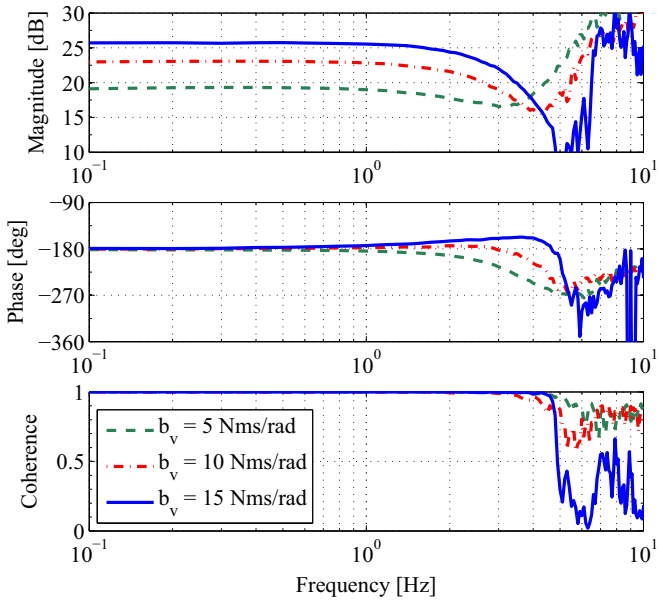

Fig. 16. Frequency response of the damping control (Spring 3).

the SEA assembled with Spring 3. The stiffness control bandwidth considering the values k_v equal to 10, 30 and 60 N m/rad is respectively 0.4, 1.4 and 2.7 Hz. Note that a larger bandwidth is achieved with higher values of k_v. This is justifiable, since the largest bandwidth is obtained when k_v is equal to k_s (approximately 105 N m/rad), and at high frequencies, the virtual stiffness value (k_v) tends to the spring stiffness (k_s).

Fig. 17(b) shows the Bode plot of the closed loop transfer function $T_k(j\omega)$ considering a constant value of virtual stiffness (k_v =60 N m/rad) for the SEA assembled with the different springs. Note that, the lower the spring constant, the higher the stiffness control bandwidth. The other results obtained are shown in Table 5.

The results, if compared with knee joint dynamic properties presented in the literature Zhang, Nuber, Butler, Bowen, and Rymer (1998), show that the proposed rotary SEA is able to render a desired stiffness and damping within a range of appropriate amplitude and frequency to assist the knee joint.

Table 5
Stiffness control bandwidth.

Spring	Bandwidth (Hz)		
	k_v=10 N m/rad	k_v=30 N m/rad	k_v=60 N m/rad
1	0.6	1.5	3.8
2	0.5	1.4	2.9
3	0.4	1.3	2.5

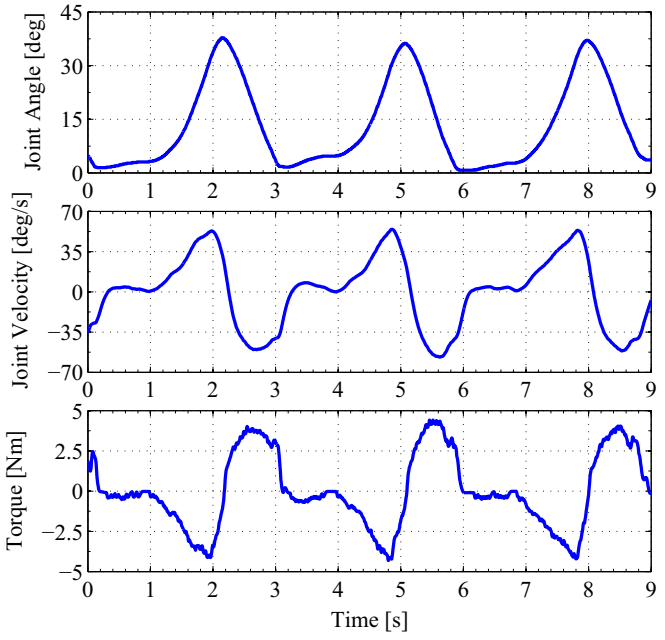

Fig. 18. Experimental data of active orthosis during walking when the desired torque is set to zero (Spring 3).

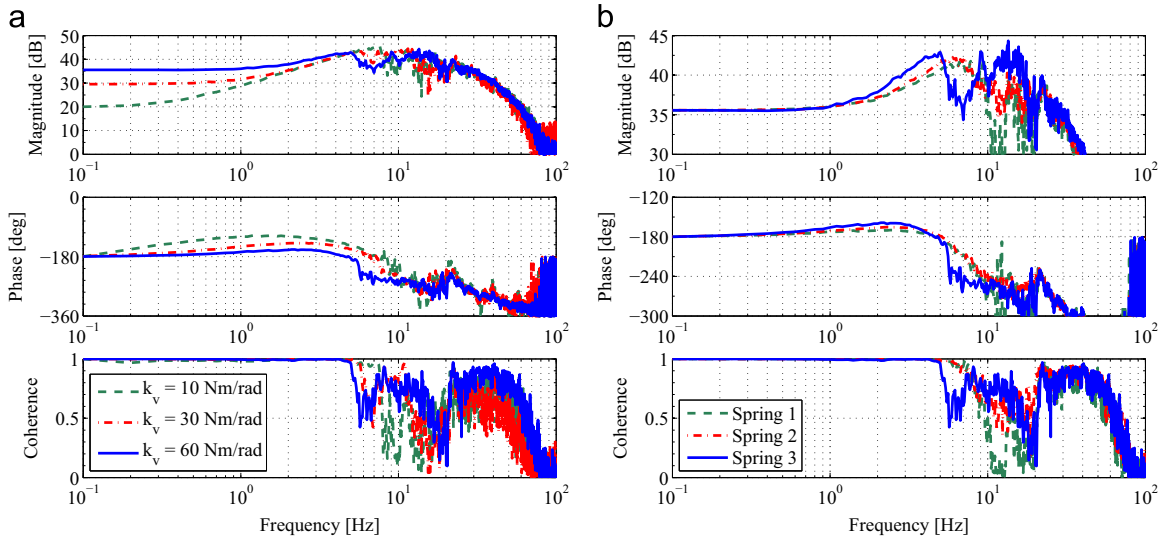

Fig. 17. Frequency response of the stiffness control. (a) (Spring 3). (b) (k_v=60 Nm/rad).

Please cite this article as: dos Santos, W. M., et al. Design and control of an active knee orthosis driven by a rotary Series Elastic Actuator. *Control Engineering Practice* (2015), http://dx.doi.org/10.1016/j.conengprac.2015.09.008

5. Experimental results with active knee orthosis

5.1. Torque control

According to Kong et al. (2009), to perform a good torque control in robots interacting with humans, an accurate actuation system with low impedance is desired. In other words, the active orthosis must follow the knee joint motion, so that the subject does not feel any resistance, when the desired torque is set to zero. Therefore, the following experiment was performed: one subject walked on a treadmill using the active knee orthosis with the desired torque set to zero.

As expected, the SEA followed the human joint motion to keep zero spring deflection. Fig. 18 shows the angle and velocity of the knee joint and the interaction torque between the user's limb and the active orthosis, for a gait cycle duration of 3 s. Note that the resistive torque generated by the actuator is proportional to the joint angular velocity. This is due to the presence of an intrinsic damping in the actuator. The active knee orthosis works as a damper when the desired torque is set to zero. Note also that the stability was not affected by the human motions.

The active knee orthosis was also commanded to track a torque profile defined as a sine wave with amplitude of 6 N m and frequency of 0.1 Hz in order to evaluate accuracy and robustness of the adopted control strategy while interacting with a human. Fig. 19(a) shows knee joint angle, reference and actual torque as well as magnitude of the torque error when the subject resists the generated torque. The subject is able to resist the applied torque, maintaining a near zero joint position. The root mean square (rms) value of the torque error is 0.1 N m, demonstrating that the active orthosis is able to generate the desired torque accurately. Fig. 19 (b) shows knee joint angle, reference and actual torque, and magnitude of the torque error when the subject is complaint with the generated torque. The rms value of the torque error is 1.06 N m. The torque error shown in Fig. 19(b) is greater than that shown in Fig. 19(a) because of the human motion. However, it must be noted that the stability was not affected.

5.2. Impedance control

As a preliminary validation of the impedance control, the active orthosis was commanded to track a knee joint trajectory profile with low and high impedance, the controller's stiffness parameter

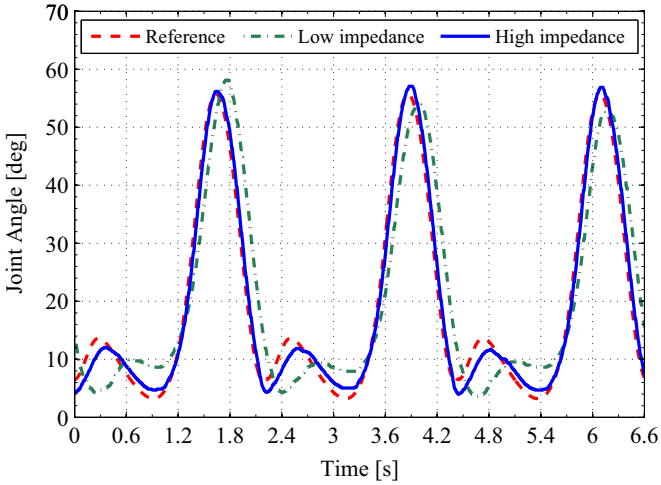

Fig. 20. Experimental data of active orthosis during walking with low and high impedance (Spring 3).

was adjusted, respectively, to 20 and 100 N m/rad. In both cases, the virtual damping was set to zero. The trajectory profile was computed by interpolation of several points of a normal gait obtained in Kirtley (2006), for a gait cycle duration of 2.2 s, Fig. 20. Note that the higher the stiffness value, the greater the accuracy will be.

5.2.1. Variable impedance control strategy

In this section, a variable impedance control strategy is evaluated, where two different values of the virtual stiffness are defined for the stance and swing phases of the gait cycle, $K_1 = 100$ and $K_2 = 25$ N m/rad, respectively. For simplicity, in both cases, the virtual damping was set to zero. At the first moment, a subject wearing the knee orthosis and walking on a treadmill was asked to follow the orthosis trajectory without imposing constraint to its movement. In the second moment, the subject was asked to force the device against the desired trajectory, trying to modificate it.

These tests were proposed to show the orthosis ability to perform variable impedance during the gait phases. This feature will be useful in our on-going efforts to design adaptive impedance control strategies for robot-aided rehabilitation. For example, in Ibarra, Santos, Krebs, and Siqueira (2014) the robot's stiffness is

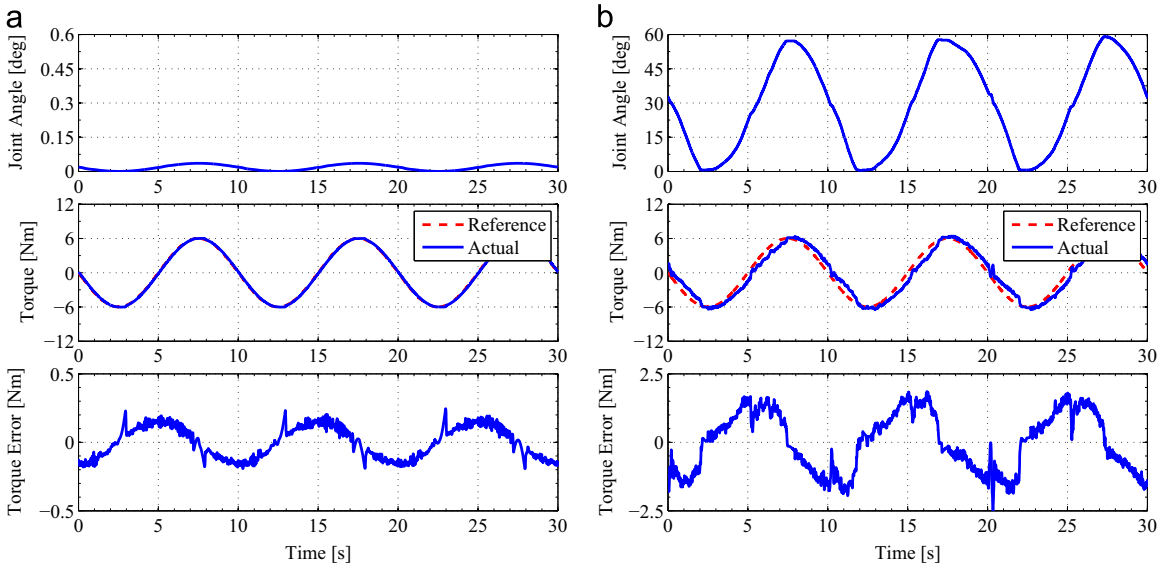

Fig. 19. Experimental data of active orthosis when the desired torque is set as a sinusoidal wave (Spring 3). (a) With movement constraint. (b) Without movement constraint.

Please cite this article as: dos Santos, W. M., et al. Design and control of an active knee orthosis driven by a rotary Series Elastic Actuator. *Control Engineering Practice* (2015), http://dx.doi.org/10.1016/j.conengprac.2015.09.008

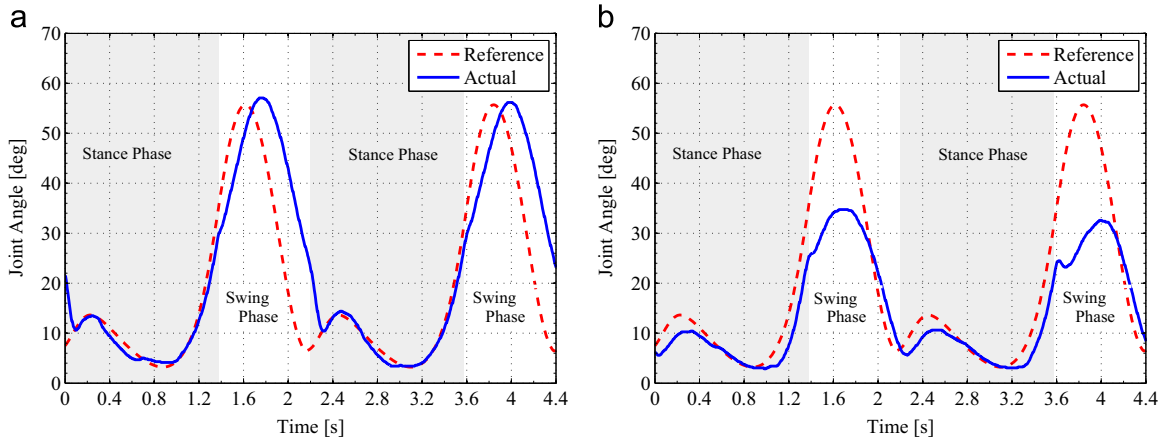

Fig. 21. Analysis of the variable impedance control (Spring 3). (a) Variable impedance without external torque. (b) Variable impedance with external torque.

adjusted based on the patient's stiffness estimation and on her/his performance on playing distinct video games. The same approach is now under investigation for walking conditions.

Fig. 21(a) shows the active orthosis behavior in the absence of external torque, when there is no movement constraint. It is possible to note that the reference trajectory is followed by the orthosis in the two different impedance states (K_1 and K_2). On the other hand, when a torque is applied by the subject against the desired trajectory, Fig. 21(b), the reference trajectory is followed only in the highest impedance state, K_1. In this case, the applied torque by the orthosis compensates the external torque and guarantees the trajectory tracking. However, in the low impedance state, K_2, the torque decreases and the reference trajectory is not followed, allowing the user to move the orthosis easily out of the desired trajectory.

6. Conclusions

This paper presents the design of an active knee orthosis driven by a customized rotary Series Elastic Actuator to assist in flexion/extension of the knee joint during physical therapy. A customized torsion spring is designed through simulations based on finite element method with the aim of fulfilling a set of requirements defined in terms of admissible peak load, low stiffness and a compact and lightweight design. The value of the spring constant determined experimentally is significantly lower than obtained by simulations. This discrepancy is probably due to the actual properties of the material being different from the nominal used in the simulation and the imperfections in the model and mesh used in the analysis. The resulting mass of the rotary SEA is 2.5 kg, thus allowing direct mounting of the actuator on the frame of a knee orthosis.

Torque and impedance controllers are implemented to ensure secure interaction with the patient, enabling new strategies for rehabilitation, for example, a variable impedance control strategy is performed and shows that it is possible to regulate the impedance during walking. The performance of the controllers was evaluated through frequency response analysis. The adopted torque control strategy, based on $\mathcal{H}_\infty$ criterion, allows the rotary SEA to provide a continuous torque of 5 N m with a bandwidth of 9.6 Hz. The results obtained for impedance control show that the actuator is able to render a desired stiffness and damping within a range of appropriate amplitude and frequency to assist the knee joint. A comparison of the proposed $\mathcal{H}_\infty$ controller with similar controllers designed for rehabilitation are under investigation.

Experiments, involving the interaction between a subject and the active orthosis, were performed in order to evaluate the performance of the developed prototype. The initial results showed in this paper are part of our on-going efforts to design adaptive impedance control strategies for robot-aided rehabilitation. A clinical study with patients will be conducted in future works to evaluate if the proposed orthosis is more effective than other available devices.

Appendix A. Supplementary data

Supplementary data associated with this paper can be found in the online version at http://dx.doi.org/10.1016/j.conengprac.2015.09.008.

References

Carpino, G., Accoto, D., Sergi, F., Tagliamonte, N. L., & Guglielmelli, E. (2012). A novel compact torsional spring for series elastic actuators for assistive wearable robots. *Journal of Mechanical Design*, *134*(12), 1–10.

Ferris, D. P., Sawicki, G. S., & Domingo, A. (2006). Powered lower limb orthoses for gait rehabilitation. *Topics in Spinal Cord Injury Rehabilitation*, *11*(2), 34–49.

Ham, R. V., Sugar, T. G., Vanderborght, B., Hollander, K. W., & Lefeber, D. (2009). Compliant actuator designs. *IEEE Robotics Automation Magazine*, *16*(3), 81–94.

Hogan, N. (1985). Impedance control: An approach to manipulation. *Journal of Dynamic Systems Measure Control, 107*(Parts 1–3) (1), 1–24.

Ibarra, J. C. P., Santos, W. M., Krebs, H. I., & Siqueira, A. A. G. (2014). Adaptive impedance control for robot-aided rehabilitation of ankle movements. In *5th IEEE RAS & EMBS international conference on biomedical robotics and biomechatronics* (pp. 664–669), São Paulo, Brazil.

Kirtley, C. (2006). *Clinical gait analysis: Theory and practice* (1st ed.). Philadelphia, PA: Elsevier Churchill Livingstone.

Kong, K., Bae, J., & Tomizuka, M. (2009). Control of rotary series elastic actuator for ideal force mode actuation in human robot interaction applications. *IEEE/ASME Transactions on Mechatronics*, *14*(1), 105–118.

Kong, K., Bae, J., & Tomizuka, M. (2012). A compact rotary series elastic actuator for human assistive systems. *IEEE/ASME Transactions on Mechatronics*, *17*(2), 288–297.

Kwakkel, G., Kollen, B. J., & Krebs, H. I. (2008). Effects of robot-assisted therapy on upper limb recovery after stroke: *A systematic review. Neurorehabilitation and Neural Repair*, *22*(2), 111–121.

Lagoda, C., Schouten, A., Stienen, A., Hekman, E., & van der Kooij, H., (2010). Design of an electric series elastic actuated joint for robotic gait rehabilitation training. In *Proceedings of 3rd IEEE RAS and EMBS international conference on biomedical robotics and biomechatronics* (pp. 21–26), Tokyo, Japan.

Maia, N. M. M., & Silva, J. M. M. (1997). Theoretical and experimental modal analysis. Engineering dynamics series. Research Studies Press Limited, Baldock, Hertfordshire, UK.

Prange, G. B., Jannink, M. J. A., Groothuis-Oudshoorn, C. G. M., Hermens, H. J., & Ijzerman, M. J. (2006). Systematic review of the effect of robot-aided therapy on recovery of the hemiparetic arm after stroke. *Journal of Rehabilitation Research and Development*, *43*(2), 171–183.

Pratt, G., & Williamson, M. (1995). Series elastic actuators. In *Proceedings of the 1995 IEEE/RSJ international conference on intelligent robots and systems* (Vol. 1, pp. 399-406), Pittsburgh, USA.

Robinson, D. W. (2000). Design and analysis of series elasticity in closed-loop actuator force control (Ph.D. thesis). Cambridge: Massachusetts Institute of Technology.

Robinson, D. W., Pratt, J. E., Paluska, D. J., & Pratt, G. A. (1999). Series elastic actuator development for a biomimetic walking robot. In *IEEE/ASME international conference on advanced intelligent mechatronics* (pp. 561–568), Atlanta, USA.

Santis, A. D., Siciliano, B., Luca, A. D., & Bicchi, A. (2008). An atlas of physical human robot interaction. *Mechanism and Machine Theory*, *43*(3), 253–270.

Santos, W. M., & Siqueira, A. A. G. (2014). Impedance control of a rotary series elastic actuator for knee rehabilitation. In: *19th World congress of the international federation of automatic control* (pp. 4801–4806), Cape Town, South Africa.

Sergi, F., Accoto, D., Carpino, G., Tagliamonte, N. L., & Guglielmelli, E., (2012). Design and characterization of a compact rotary series elastic actuator for knee assistance during overground walking. In *The Fourth IEEE RAS/EMBS international conference on biomedical robotics and biomechatronics* (pp. 1931–1936), Roma, Italy.

Skogestad, S., & Postlethwaite, I. (2005). *Multivariable feed back control: analysis and design* (2nd ed.). NewYork: John Wiley and Sons.

Stienen, A. H. A., Hekman, E. E. G., ter Braak, H., Aalsma, A. M. M., van der Helm, F. C. T., & van der Kooij, H. (2010). Design of a rotational hydroelastic actuator for a powered exoskeleton for upper limb rehabilitation. *IEEE Transactions on Biomedical Engineering*, *57*(3), 728–735.

Tsagarakis, N., Laffranchi, M., Vanderborght, B., & Caldwell, D., (2009). A compact soft actuator unit for small scale human friendly robots. In *Proceedings of IEEE international conference on robotics and automation* (pp. 4356–4362), Kobe, Japan.

Wyeth, G. (2006). Control issues for velocity sourced series elastic actuators. In *Proceedings of the Australasian conference on robotics and automation* (pp. 1–6), Auckland, New Zealand.

Yoon, S. S., Kang, S., Yun, S. K., Kim, S. J., Kim, Y. H., & Kim, M. (2005). Safe arm design with mr-based passive compliant joints and viscoelastic covering for service robot applications. *Journal of Mechanical Science and Technology*, *19*(10), 1835–1845.

Zhang, L. Q., Nuber, G., Butler, J., Bowen, M., & Rymer, W. Z. (1998). In vivo human knee joint dynamic properties as functions of muscle contraction and joint position. *Journal of Biomechanics*, *31*(1), 71–76.

Please cite this article as: dos Santos, W. M., et al. Design and control of an active knee orthosis driven by a rotary Series Elastic Actuator. *Control Engineering Practice* (2015), http://dx.doi.org/10.1016/j.conengprac.2015.09.008